

# A design, mechanical rating and load adaptation method for cellular components for additive manufacturing

Tobias Ziegler<sup>1\*</sup>, Raimund Jaeger<sup>1</sup>, Christof Koplin<sup>1</sup>

Fraunhofer Institute for Mechanics of Materials IWM, Wöhlerstraße 11, 79108 Freiburg

\*Corresponding author, tobias.ziegler@iwm.fraunhofer.de

## Abstract

We present a tool for lightweight construction by internally structuring bulk volumes for the Design for Additive Manufacturing (DfAM). Essential to cost efficient, rapid prototyping is a reliable assessment of mechanical properties without having to build spare samples for testing. Due to its regular nature, our structure allows a beforehand calculation of the mechanical properties like strength and stiffness, even for large geometries with many cells. To improve the mechanical performance of the entire component, the structure of the cells can be adapted in response to a pre-determined load. This adaptation is achieved by locally anisotropic increasing the diameter of selected struts. It significantly enhances the load bearing capacity of the product with a low increase in material and production time.

For the parameterization of finite element calculations, tests on only a few structured representative specimens are necessary to model the material used in the additive manufacturing process. We have performed the necessary experiments and developed a homogenized material model for a structure made up of polyamide 12, which is used in Selective laser sintering (SLS) and offers specific strength comparable to steel. To prove the viability of the layout and rating method we structured, manufactured and tested one life size cantilever chair.

The approach presented in this paper can be applied to a large variety of component shapes to assess and improve the mechanical capacity of a cellular structure based on how a few cells of a small volume perform.

## Keywords

Additive Manufacturing, Homogenization, Cellular Structures, Optimization, Design for additive Manufacturing

## 1. Introduction

Additive manufacturing allows for individual designs with controllable structures. A systematic approach is highly desirable for assessing the design and especially the mechanical performance of an additively manufactured complex in the design phase. On the one hand, building large, complex structures by additive manufacturing is still costly; as a result, it is desirable that a prototype exhibits already the required mechanical properties. On the other hand, additive manufacturing facilitates the production of components in small quantities – even the production of individually designed components remains economically feasible. Long cycles of producing and testing spare specimens are not desirable. We present a method of generating cellular structures within the outer shape of a bulk Computer Aided Design (CAD) whose stiffness and strength we can calculate by Finite Element Modeling (FEM). The method also allows to automatically adjust the diameter of concerned struts to one prevalent load case, to increase the load bearing capacity while still being a lightweight design and retaining resilience against deviations from this load case. Possible applications are medical implants, Insoles, designer furniture or lightweight parts for aerospace.

### 1.1. Cellular Structures

Cellular structures make lightweight designs and although they are not ideal for a single load case more cells are less sensitive to imperfections (Bruns 2005). This is especially desirable for additive manufacturing as produced parts vary in their quality because of surface roughness and deviations in the temperature field. Furthermore, if a cellular structure is loaded in an unforeseen way more struts keep a higher stiffness and strength compared to fewer struts of greater diameter (Gibson 2005). This implies a greater resilience against variations in the load. For additive manufacturing, cellular structures allow the designer to integrate different stiffness while using just one material. We based the cellular structure on a trabecular structure similar to the one found in cancellous bone and similar to a structure proposed by Kowalczyk (2003) (see Figure 1). We can adapt these structures to a given load, thus employing a biomimetic approach (Fratzl 2007) by a local, increase of the diameter of selected struts. It significantly enhances the load bearing capacity of the product with a low increase in material and production time. Due to its regular structure, this cell allows a beforehand calculation of mechanical properties like strength and stiffness.

### 1.2. Homogenization

To reduce the computing time we have employed a homogenization scheme that vastly reduces the number of nodes the equations have to be solved for. Thus our design permits to mechanically rate large and complicated structures with many cells. Instead of having a detailed mesh for the cellular structure we regard each cell as one element thus saving on the time required for computing stresses and strains. For the parameterization of finite element calculations, tests on

only a few representative specimens are necessary to model the material used in the additive manufacturing process. One can apply this Homogenization to any material used in additive manufacturing and most processes available. Limitations occur because of the cellular structure which cannot be produced for example in layered object manufacturing, as the negative parts cannot be removed. Overhangs require large amounts of supporting structure in processes like Fused Deposition Modelling or Inkjet Printing. We have concentrated on Selective laser sintering (SLS), when changing the process or the material new tests are required.

### 1.3. Methodology

Our methodology to generate conformal load adapted cellular structures is described below. An detailed example of the method will be given below when discussing the demonstrator.

- a) **Given outer shape:**  
Typically the outer shape of a component is given as a CAD file.
- b) **Conformal meshing with Solid Hex Elements:**  
The component is meshed with solid hex elements like it would be done for a standard FEM-step. We have employed Hypermesh to generate the hex-mesh but other mesh-generators are available on the market. The method is currently limited to hex-elements. Other shapes might be added later.
- c) **Definition of load case:**  
The load case typically comes from the application. This is defined like it would be done for a standard FEM-step
- d) **FEM with homogenized Material data for simple cellular structure:**  
We have employed the ABAQUS (2011) simulation code and the associated file format. We determined homogenized material properties for a simple cellular structure made from PA12 by selective laser sintering experimentally.
- e) **Picking simple/strengthened unit cell from library:**  
According to the results from the previous FEM step a unit cell is picked from a library. For this publication the stress at the center of each Element was transformed along the strut direction and evaluated by an automated Abaqus Python script. The deduction criteria can be easily implement as the whole range of results available from FEM can be employed. Additional unit cells can easily be added to the library.
- f) **Replacing each FE-Element by chosen unit cell:**  
A unit cell from the library (in the Abaqus mesh format) is taken for each element and sized, rotated and deformed according to the replaced element. This ensures a perfect fit of the struts at each element face and allows for a closed element at the outer surfaces of the component. This step is automated by a self-developed Python software called StlInsert.
- g) **Repetition of FEM with updated Material properties:**  
For an iterative optimization the FEM-step d) can be repeated with updated material properties according to the chosen unit cell. This step is automated by the Abaqus Python script from step e).
- h) **Writing of .stl file:**  
A .stl file is exported by StlInsert that can be produced by most additive manufacturing machines. A special emphasis was put on file size, as for most complex cellular structures a geometric representation can easily exceed the possibilities the machines.

## 2. Literature

### 2.1. Homogenization

The oldest homogenization approach is the mean field approximation (MFA) proposed by Hill (1963). The MFA averages the microscopic stresses and strains over the respective volumes which gives the macroscopic values. The average should be done over a representative volume element (RVE) which should be so large that the average field values do not change if the RVE is increased. On the other hand, the RVE should be smaller than macroscopic component dimensions. The beauty of this MFA is that one can obtain the microscopic stresses by any method available. For simple geometries this can be done analytically or a numerical model can be used like FEM. The MFA has been compared by Hori and Nemat-Nasser (1999) with what they call the “homogenization theory”. This theory calculates the macroscopic fields by using a perturbation approach. They developed a hybrid theory from these two approaches towards homogenization, assuming linear elastic properties can be used and that the length scales of the macroscopic body are orders of magnitude greater than the microscopic length scales. The cellular structures considered in this paper present a subset of these general theories where one component (the void) has a vanishing stiffness. Different orientations of particles (in our case voids) within a surrounding medium were considered by Nunan and Keller (1984).

## 2.2. Generating cellular structures

There are a number of comparable schemes of generating cellular structures known in the literature: Petrovic et al. (2010) investigated the influence of different types of base cells on the mechanical behavior of a structured component. They did not adjust the cell geometry and orientation according to the local stresses by doing so. The approach mentioned by Chen (2006) focuses on structuring the surface of a component with struts, again without optimizing them for their mechanical behavior. These solutions are process dependent. The fused deposition and other material extrusion processes create tool paths that can generate very weak structures. Both publications mention the problem of generating large amounts of data that have to be processed for production. Cook et al. (2010) have presented an »Onion-Skin Approach« where FEM calculations give the load on a component. The component is then split into skins of similar load which are then filled with base cells whose density is matched to that load. The structure is optimized iteratively. However, the orientations of the internal skin-interfaces are not adjusted according to the direction of the flux of force. The complexity of these Onion-Skins limits the applicability of simulations and the use for arbitrary components. A similar approach was presented by Rosen (2007) where a sheet part was filled by struts whose diameter was adjusted according to a predetermined load. To reduce computational cost struts were clustered into parts and all struts within a cluster had the same diameter. The method for generating structures by Teufelhart and Reinhart (2012) generates struts that follow the flux of force. The struts are then adjusted with respect to loads. This gives well-adjusted structures for the price of getting very complex geometries, even for simple components with simple load cases. With their geometry at the connection points of the struts high notch stresses occur.

Ponche, Kerbrat, Mognol and Hascoet (2014) go a step further and developed methodology for generating internal structures that takes into account physical phenomena of the specific manufacturing process. For an additive laser manufacturing process they optimized the path of the process for thin-walled objects like a turbine blade.

## 2.3. Experimental characterization of material

Laser sintering of PA12 is a complex process that can yield very different mechanical results. The strength is influenced by the process parameters, firstly the amount of energy put into the system per area as observed by Caulfield (2007). He recommended for his parameters a laser power of at least 11 W and obtained best values for yield strength, tensile strength and stiffness for 18 W. But also the scan strategy influences the strength as observed by Kaddar (2010). Parallel scanlines along the x- and y- direction can lead to a difference in strength of up to 7% due to different cooling times. Parameters like the hatch distance and single or double scan further influence the strength and stiffness of PA12 from SLS. Also the mere position within the build chamber can influence strength and stiffness due to different temperatures within the machine as described by Goodridge (2012). Over all the density seems to be a critical parameter for the mechanical properties as witnessed by Van Hooreweder (2010). Lastly an anisotropy between tensile and compressive loading of PA12 from SLS has been observed by Ajoku (2006) with compression achieving higher strength.

### 3. Experimental

Rpm GmbH produced the test specimens of the base cell from polyamide 12 (PA12) named Orgasol (see Figure 1 for an example). These were made by selective laser sintering on a DTM Sinterstation with a laser power of 16 W. These cells fill a volume fraction of 16 % and the struts have a cross-section of around 6 % of the area. We tested four specimens each under different loading setups, i.e. compressive, tensile and shear loading. We separated these specimens in two setups: one with the loading direction being perpendicular to the building direction (called ‘T’) and the other with both being collinear (called ‘II’). All experiments were done quasi-statically on a MTS calibrated testing machine under displacement control at a speed of either 0,5 mm/min or 0,75 mm/min. The resulting forces were recorded as well as the displacement of the fixation. Due to the low stiffness of the specimens compared to the rigid steel fixation no displacement or strain measure on the specimen was deemed necessary. The results for the compressive tests are given in Table 1.

**Table 1** Compressive loading, experimental results on Young’s moduli and Strength of cellular specimens made from Orgasol plastic material

| Specimen                              | Young’s modulus [MPa] | Strength [MPa]  | Full material (PA12) Young’s modulus estimated [MPa] | Full material (PA12) Strength estimated [MPa] |
|---------------------------------------|-----------------------|-----------------|--|---|
| Orgasol T                             | $60,0 \pm 4,5$        | $1,96 \pm 0,25$ | 822  | 51,7  |
| Orgasol II                            | $72,5 \pm 9,7$        | $2,63 \pm 0,03$ | 993  | 69,4  |
| <i>Hashin-Shtrikman</i>               | <i>151,8</i>          |                 |  |   |
| <i>Full material by Schmid (2015)</i> |                       |                 | <i>1800</i>  | <i>45</i>                                     |

Additionally the analytical upper bound by Hashin and Shtrikman (1963) for a composite with 16 % PA12 (Young’s modulus of 1500 MPa) and 84 % air are given. For the full material data, we used FEM analysis, which showed that a full block would have 13.7 times the stiffness of this cell geometry. The highest stress concentration for the cell geometry was 26.4 times the stress it would have been for a full block which we used to estimate the strength. These rough estimates for the full material are compared to the results given by Schmid (2015). We did a similar set of experiments under tensile loading condition (Table 2).

**Table 2** Tensile loading, experimental results on Young’s moduli and Strength of cellular specimens made from two different plastic materials

| Specimen   | Young’s modulus [MPa] | Strength [MPa]  |
|------------|-----------------------|-----------------|
| Orgasol T  | $47,6 \pm 7,1$        | $1,28 \pm 0,11$ |
| Orgasol II | $45,1 \pm 3,3$        | $0,59 \pm 0,42$ |

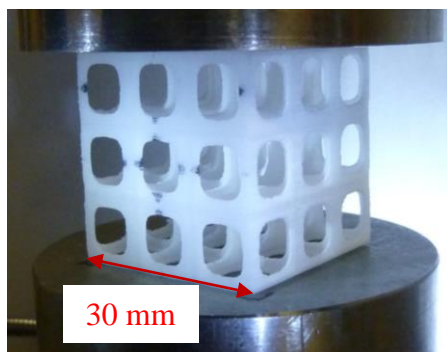


**Figure 1:** Cellular test specimen with a 30 mm base length under compressive load

### 4. Homogenization

We homogenized the resulting component stiffness and load bearing capacity to assign values for Young’s modulus and plastic flow to just one base cell. The advantage of this homogenization is the large reduction in computational time during simulations. The computing time of a FEM scales with  $n^a$  where  $n$  is the number of nodes and  $2 < a < 3$

depending on the implementation. The substitution of a finely meshed structure with a homogenized volume element reduces the number of nodes by a factor of 750 for the base cell used.

To account for the different strength in tension and compression we used the material model by Hjelm (1992) as implemented in ABAQUS (2011). This model has been applied to cast iron, which also exhibits anisotropy between tension and compression. The fit we used is shown in Figure 2. One assumes that the elastic constants under tension and compression are the same by using this model. We used the average of the values for compression and tension. Under compression the stress-strain-behavior (black) was found to bend slightly backwards while under tension it was found to bend slightly forward above the origin.

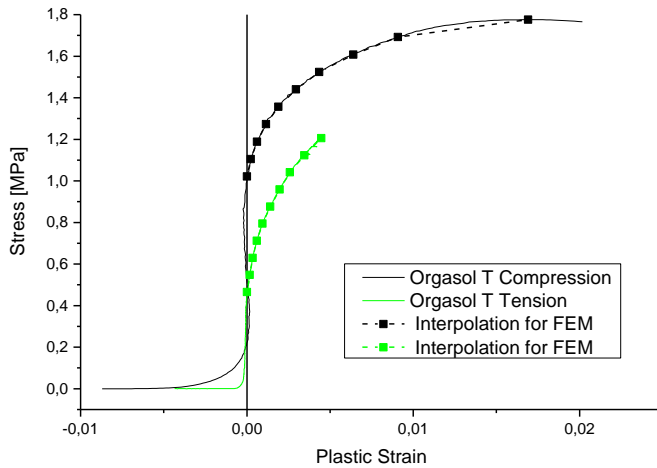


**Figure 2** Experimental stress vs plastic strain curves for Orgasol T under compression and tension as well as the interpolated fit for the homogenized FEM model

To validate the homogenization for different loading situations we carried out shear tests (Figure 3) and bending test (Figure 4) and compared these to simulations that used the homogenized material model from Figure 2. The cube specimens had to be embedded into a fixation material at the sides for the shear tests. This was necessary as the specimens themselves would wind out of their fixations during testing. To obtain deformation curves we used an optical measurement system where a computer continuously identifies specific points in images from the setup and tracks their movement during the experiment (red points in Figure 3 left are searched and found within the green squares). From this data we calculated the deformation for two diagonals going down (Top Left to Bottom Right) and up (Bottom Left to Top Right). We modeled a similar setup with the homogenized material data and the resulting curves can be compared in Figure 3 Right. The predicted strength and stiffness were greater than observed experimentally (292 N versus 249 N).

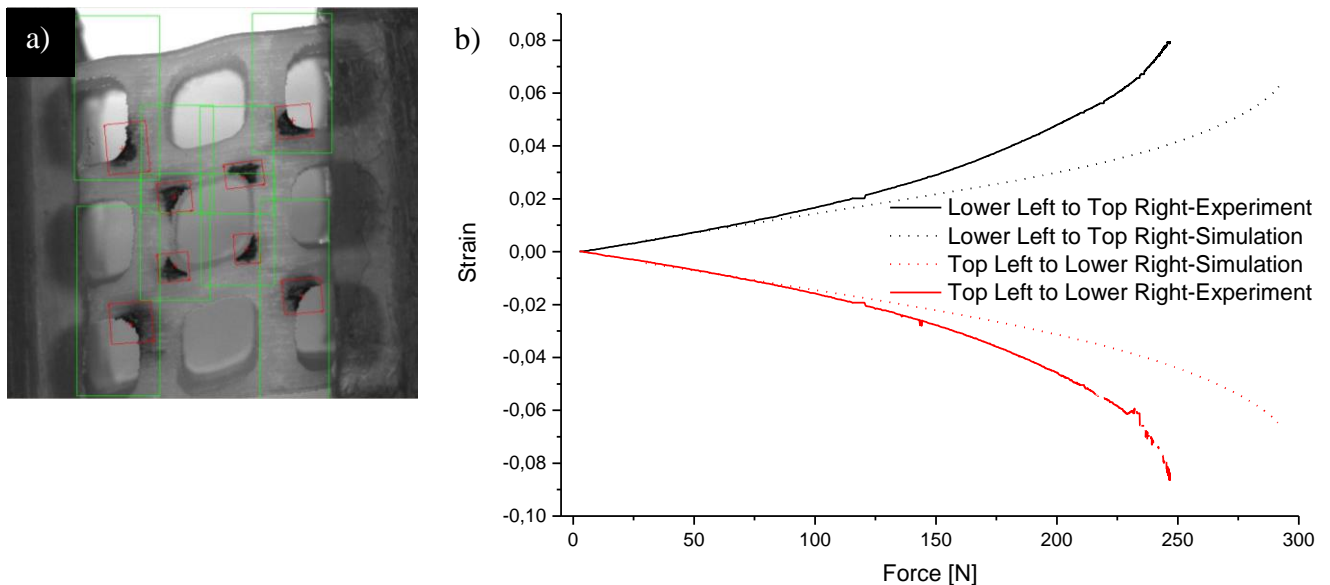


**Figure 3 a):** Computer Image from an experimental shear test. The deformation was measured optically by a computer identifying the red points within the red and green squares and tracking their movement.

**b):** Comparison of experimental and simulated shearing curves of the homogenized model

For further validation we chose the bending setup because a bending bar features areas of compressive as well as tensile loading. The resulting Force-Deflection curve was compared to data obtained by simulation using the homogenized material data (Figure 5). The FE-simulation is conducted beyond the strength of the material. Therefore, we had to cut off the simulation when the maximum plastic strain at the top of the bending bar reached a value higher than was found in the experiment. The simulation was able to predict the Force-Deflection curve adequately and the deformation behavior matched that observed in the experiment, including the caving at the lower roller (Figure 4). The bending bar failed under tensile loading and shattered in many pieces.

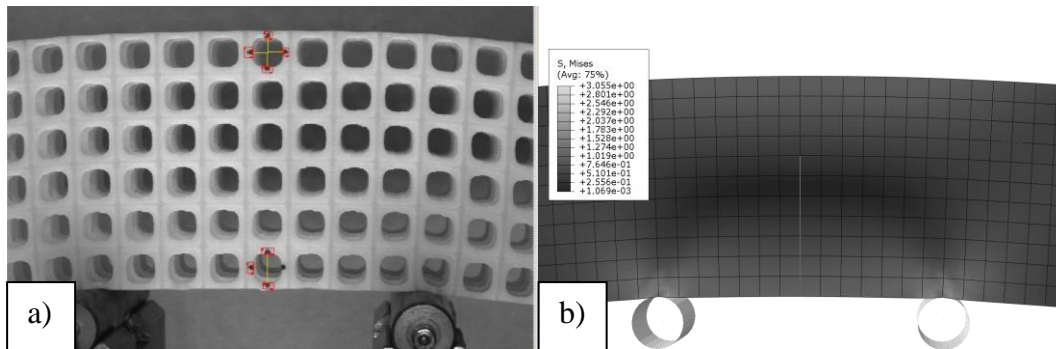


**Figure 4 a):** Bending specimen subjected in different regions to compressive, tensile and shear loading.  
**b):** Homogenized model with input data gathered from earlier experiments

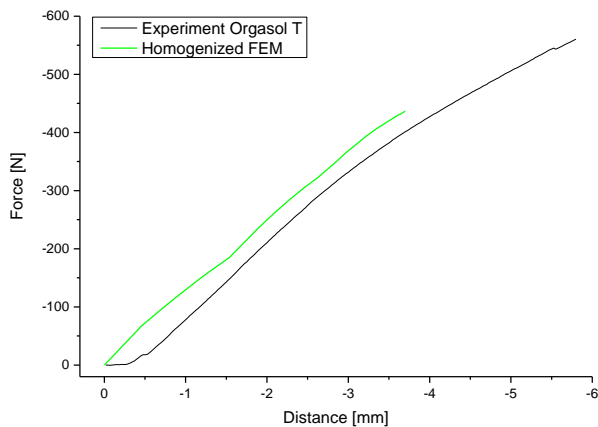


**Figure 5** Comparison of experimental and simulated Force-Deflection curve for a Bending specimen. Homogenized material data were used for the simulation

So far only rectangular components have been tested and modeled. In order to qualify this homogenization also for curved components we have structured bending bars whose far faces stand at different angles ( $0^\circ$ ,  $10^\circ$ ,  $20^\circ$ ,  $30^\circ$ ,  $40^\circ$  and  $50^\circ$ ) to each other. For each angle rpm GmbH manufactured three specimens that we tested for their stiffness and ultimate strength. Additionally FE-simulations with the homogenized material data have been performed on the bend shapes to compare to the experimental results. All of these results are shown in Figure 6. For the smaller angles ( $0^\circ$  –  $30^\circ$ ) all bending bars in these experiments failed by shearing while for larger angles ( $40^\circ$  and  $50^\circ$ ) we observed a tensile failure. This is probably because the angle between the line from the outer roller to the inner roller and the vertical was close to  $45^\circ$  when deformed close to failing for the bending bars with smaller angles which favors the development of shear bands. For the bars with the larger angles the loading angle between the line from the outer roller to the inner roller and the vertical decreased to  $43^\circ$  and  $42^\circ$  when failing.

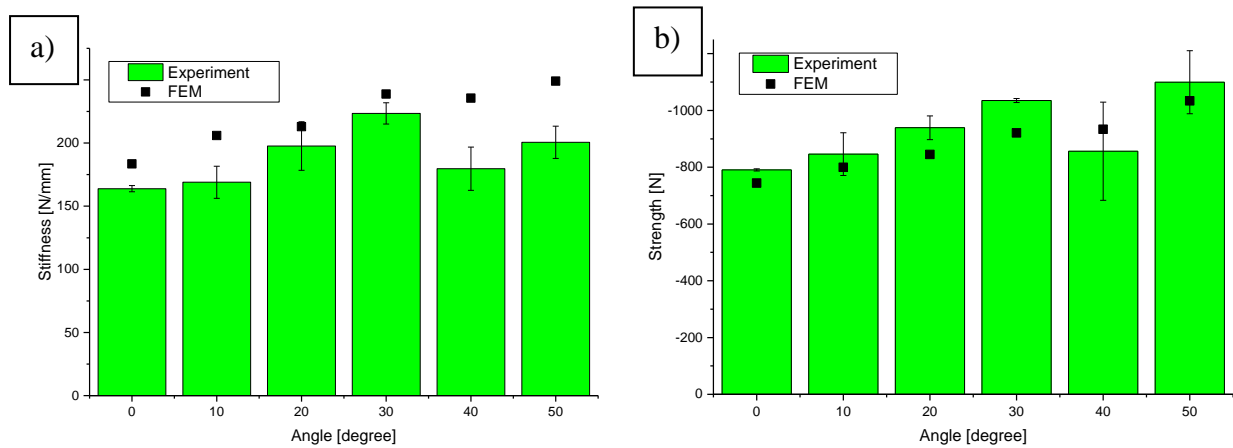


**Figure 6** Comparison of experimental and simulated stiffness **a)** and strength **b)** of bending bars with different angles between the normal of the far sides

## 5. Structuring and Adaptation

To manufacture products of different shape the meshing algorithms we used the FE-Preprocessor Hypermesh (12.0) by Altair Engineering. However, any common preprocessor can be used for the FE-Calculations and subsequently for structuring the CAD shapes. Due to its regular structure we employed cells with a hexahedron shape. However the principle could be expanded to other shapes like tetrahedrons. We created a library of cell shapes again using Hypermesh. This library consists of 12 elements that are saved in an Abaqus mesh format. Besides the cell investigated experimentally there are two steps of strengthening resulting in either a doubling of Young's modulus (dark cell in Figure 7) and strength or a fivefold increase in these values (black cell in Figure 7) with respect to the values of the base cell as shown in Figure 2. Additionally, we used three anisotropic cells (not shown) – one for each axis strengthened – for the cells in Figure 7 if the stress situation warrants these. The structure should form a closed surface in which the base cells are connected to each other. Furthermore, a smooth outer surface of the bulk CAD design has to be provided. For the structuring the software called 'StlInsert' was developed. StlInsert projects basic cell structures into the shape of irregular hex-elements like the ones used in Finite Element Analysis and connects the structure at the intersections. It follows an iterative process in which all FE-Elements are consecutively replaced by one of several cells. Due to meshing the shape of the hexahedrons might be irregular. So for each hexahedron the program calculates the center as the mean of its nodes as well as a non-Cartesian coordinate system connecting the center of opposite faces. It then loads a cell geometry from the library and transforms all nodes of that cell, that should not connect to other cells, into the coordinate system of the hexahedron, scales them accordingly and then places them at the center of the corresponding element. The nodes on the faces are treated separately in a similar fashion to assure a connection to the cell on the opposite side of the face. For each face the center is calculated and a non-Cartesian coordinate system is determined. The nodes of the cell corresponding to the face of the hexahedron are transformed by StlInsert into that coordinate system and placed at the center of that face. Additionally, for each face the size of the strut ending at that face is saved and a scaling is done if struts of different diameter meet on a face. The software then closes the faces of the hexahedrons, which do not have an opposing hexahedron, with a cap that ensures the resulting mesh is closed. The output from this software is a .stl file that can be produced by most additive manufacturing technologies. Due to rounding errors an equivalence step has to be performed at the end to make sure nodes very close to each other are merged.

For choosing a cell from the library the results from the homogenized FE-model shown in Figure 7 are automatically used. A Python script that directly reads the output of the Abaqus FE-Analysis calls the stress tensor in the centre of each element and calculates the stresses along the three axes of that element. If two of these stresses exceed the loading capacity of the basic cell, which is 0.6 MPa in tension or 1.0 MPa in compression (compare Figure 2) the Python script chooses the medium cell in Figure 7 which has double the strut crosssection compared to the light cell. If the stress is even greater the black cell in Figure 7 is used, resulting in a fivefold increase in crosssection. Additionally, if just one of the three stresses in one cell exceeds the strength of that cell an anisotropic strengthened cell is chosen. These cells had the crosssection of just one strut doubled or fivefold increased. The script saves the classification of each element into one of the 12 cells in the library within the geometry file and StlInsert interprets this information when picking a cell. All of these steps result in a geometry file in the .stl format that can be built by additive manufacturing.

As a further benefit the Python script creates input for a new FEM where the strengthening as well as the anisotropy is included in the homogenized material data. Homogenized material data for these strengthened cells were used for all modelling of macroscopic properties of strengthened structures. For these material models the stresses in Figure 2 are assumed to have double or fivefold the value from the previous experiments as do the elastic constants. For the

anisotropic cells we have made similar assumptions (i.e. a double or fivefold increase in stiffness and strength along one direction) and used anisotropic material models. To model the anisotropic behaviour the elastic properties were entered as engineering constants and the plastic flow was entered as stress ratios for anisotropic yielding. A local orientation system for the anisotropic increase for each anisotropic element was automatically written by the Python script. This allows either for an iterative optimization or a beforehand assessment of the mechanical performance of the strengthened component.

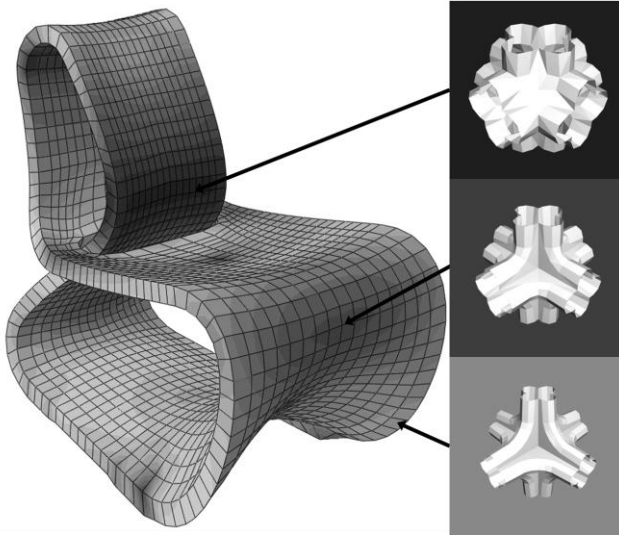


**Figure 7** Model of the Cellular Loop cantilever chair. The assumed load is a person of 150 kg sitting close to the chair-back. Different types of cells are used in different areas according to the stress present

## 6. Case Study

To demonstrate the practicability of the structuring and mechanical optimization, we chose a cantilever chair. The mechanical construction of a cantilever chair is a challenge due to their high bending loads. Famous examples of cantilever chairs are the MR20 from Ludwig Mies van der Rohe, the Panton chair and the Beast by Neri Oxman (2011). Prof. Anke Bernotat (2013) created a novel design of a cantilever chair called »Cellular Loop« at the Folkwang University of the Arts (see Figure 7, Figure 9 and Figure 10). The design is unique in that it forms a closed loop, thereby visualizing the possibilities of additive manufacturing on a larger scale. This is further emphasized by the cellular structure that would be impossible to manufacture by other means. We used a model of the chair to estimate the load bearing capacity of the chair again, using the homogenized input data from the previous section. Two load cases were studied:

1. A person of 150 kg sitting close to the chair-back
2. A weight of 30 kg pressing horizontally against the chair-back

The resulting stresses for load case 1 are plotted in Figure 7. The obtained stresses were not only used for predicting the mechanical performance like done in Figure 3 through Figure 6 but was further used to adapt the structure to the load as described in the previous section. FEM showed an increase in carrying capacity for this chair from 140 kg (**Figure 8 a**) to 400 kg (**Figure 8 b**) due to this selective strengthening of the structure.

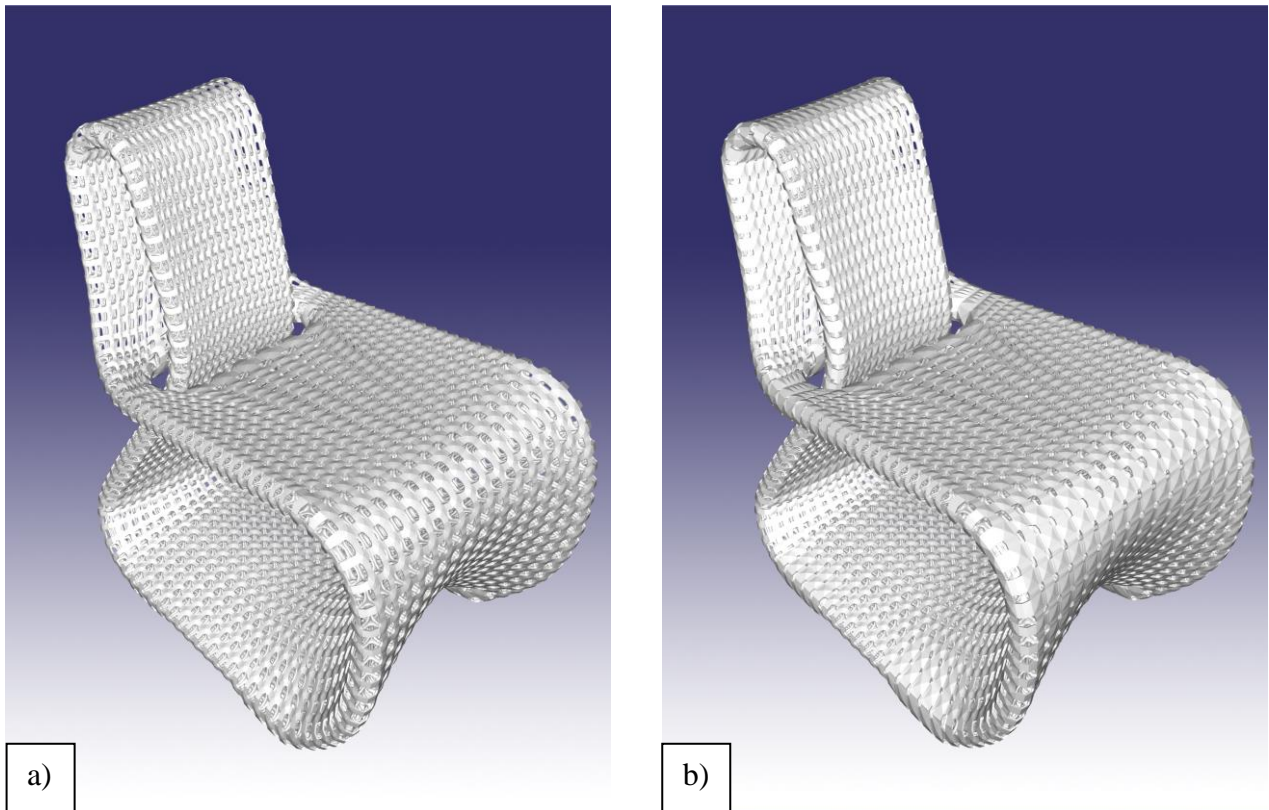


**Figure 8** stl representation of the cellular chair: a) unstrengthened version b) strengthened version  
Strengthening took place in the back rest, the knee area and around the foot of the chair.

Rpm GmbH produced a 40 % scale model of the strengthened chair that we used for testing (Figure 9). To check the increase in strength by the adaptation the model was experimentally loaded to 450 N. This load was above the load bearing capacity of an unstrengthened chair of 177 N (for the scale model) and we used this to verify the adaptation. The simulation predicted a carrying capacity of 650 N for this model.

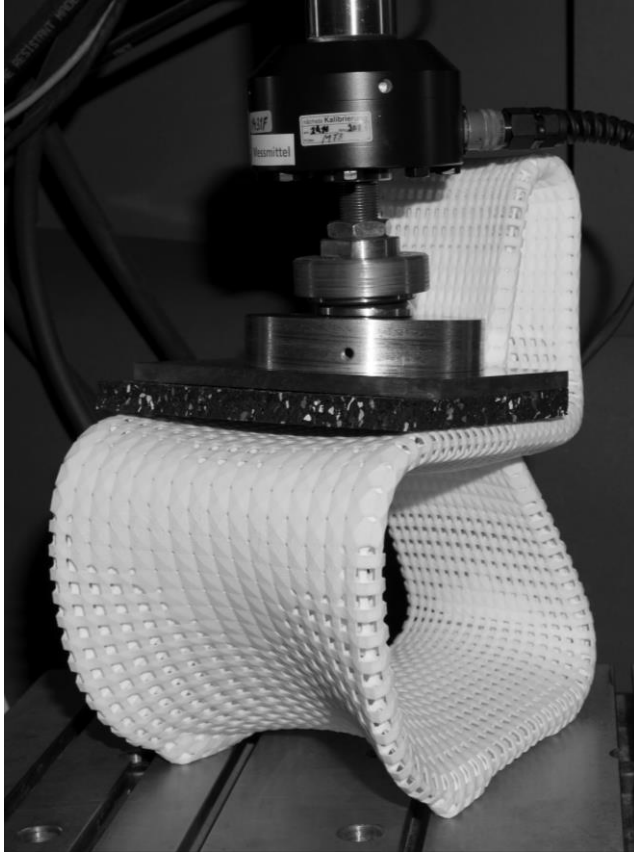


**Figure 9** Test on a small-scale (40%) model of the chair. The structure was locally adapted to the resulting stresses. Compare for example the lower back area or behind the knees where high stresses are expected with Figure 7

The life-size Cellular Loop was produced by rpm GmbH in 13 parts using a Sinterstation 2500 of DTM, USA (nowadays 3D-Systems). This required four building runs and a total of 200 hours of machine time. The parts were glued together (experiments on glued test-specimens and layout of the interfaces are not shown here) and the resulting chair is shown in Figure 10. The chair withstood people of higher weight than 140 kg above the limit of the unstrengthened structure. The file size of the final .stl was 95 MB which could be further reduced to 43 MB by zipping.

## 7. Discussion

The experimental results on the base cells in Table 1 and Table 2 show a large scatter. This might be due to size effects as the base length for the specimens was only 30 mm which results in struts that are only 3.3 mm thick. At this length scale, the resolution of the laser and the particle size of the powder might influence the mechanical properties. The Hashin-Shtrikman bound overestimates the measured compressive Young's modulus by a factor of two. This is in good agreement with the estimated stiffness from FEM, which assumes a stiffness of 7.29 % for this structure compared to the full material, which is about half of the volume fraction filled at 16 %. Or to put it in other words, only half of the material used in this structure adds to the stiffness for uniaxial compression. This shows that the cellular structure is not ideal for a single load case. The tensile strength is lower than the compressive strength. This is especially distinctive for the samples that we tested along the building direction. Ajoku, Saleh, Hopkinson, Hague, and Erasenthiran (2006) have observed this before and this keeps being one of the weaknesses of selective laser sintering of PA12.



**Figure 10** Cellular Loop chair. Photo courtesy of the Folkwang University of the Arts and Pia Kintrup, as well as Natalie Richter

The model for the material behavior used included this anisotropy under tension and compression. Under shear-loading the model overestimated the strength and the stiffness of the cell structure by roughly 20 %. As the difference in the initiation of plastic flow between tension and compression was close to 100 % and no model was available which could account for both we chose the model by Hjelm (1992). The model was able to predict the behavior of a rectangular bending bar adequately (Figure 4 and Figure 5). Here, we tested only one specimen so the discrepancy between the estimated ultimate strength (around 450 N) and the measured one (around 550 N) might be by chance. More tests were done on the curved bending bars where the ones with an angle of  $0^\circ$  correspond to the one shown in (Figure 4 and Figure 5). The estimated strength is on the conservative side as is desired for this case. For the curved bending bars the value of the estimated stiffness compares well to the measured stiffness (Figure 6). Experimentally the stiffness strongly depends on how close the loading points are to the closest struts. The simulation does not show this as the size of the rollers is close to the size of a single cell as can be seen in Figure 4 which violates the assumptions necessary for homogenization (i.e. an RVE). As the deformations are high the rollers are likely to settle in the compliant area between two vertical struts which reduces the experimental stiffness and introduces some scatter. The estimate of the strength correlates well to the measured strength (Figure 6). Generally the model underestimates the strength with the exception of the  $40^\circ$  angle where the estimate is above the measured value. Although some specimens failed under shear loading we expect the tensile failure to occur at comparable loads. We base this assumption on the fact that the bending bar shown in Figure 4 failed under tensile loading as did the curved bars with the higher angle. For  $40^\circ$  we observed a mix of tensile and shear failure. Unfortunately the model overestimates the strength under shearing. We recommend the model used only for low to medium shear stresses. If high shear stresses are to be expected a more complex model is needed to describe the plastic flow and failure of PA12 under shear loading, which was unavailable at that time.

For the medium cell in Figure 7 we have assumed that a doubling of the cross-section of the struts will also double the strength and stiffness compared to the one measured. Because of time constraints and a limited number of specimens provided we were unable to check this assumption. However, we feel confident that an increase in strut diameter should reduce the variance due to surface roughness, finite size of the laser spot and finite grain size. We have not proven the model for the strengthened data. We have verified some strengthening by testing the scale model of the chair and using the final chair which was above the limit for the unstrengthened structure.

For the Cellular Loop Chair the stress distribution shows that high loads occur at the bend at the top of the chair as well as at the forward turn of the chair-back. Within the limited number of test specimens we verified the selective

strengthening by testing one 40 % scale model of the chair above the load that a non-adapted chair could carry. Regarding the safety factors used for DfAM we have opted for a moderate conservative approach. Our strength estimates of the bending bar are below the average strength measured but not below the worst specimen measured. There are many aspects of the production process that influence the material quality. Besides the obvious influences like laser power and scanning speed there are ones that can only be controlled by the manufacturer like build orientation and refresh rate of the powder. Additionally there are more intricate ones like the deteriorating of the laser over time and the positioning within the build room and with respect to other components within that build room. Accounting for all of these is tedious and in our opinion too expensive for industrial application. For the demonstrator we chose a very conservative approach by having a safety factor of two, as we have not investigated the fatigue strength of the material.

## 8. Conclusions

A method has been presented that uses a homogenization approach for an effective simulation of the mechanical performance of cellular components without modeling them in detail. For the homogenization tensile and compression experiment have been used to parameterize the material model by Hjelm (1992) for a cellular structure made of PA12 by Selective Laser Sintering. To verify this homogenization shearing and bending tests have been done on cellular structures. While for shearing the homogenized model overestimated the strength and stiffness it was able to predict the stiffness and strength of a bending bar. This homogenization was verified to work on curved structures as well.

With the use of a Pre-processor a bulk CAD-design can be meshed into hexahedrons and FEM using the homogenized material model can predict the strength and stiffness under a chosen loading scenario. A stepwise process has been described by which a program called “StillInsert” replaces each hexahedron by a single cell. Results from FEM were used to choose the cell from a library according to the resulting stress. The algorithm automatically generates complete .stl meshes of selectively strengthened cellular structures from the FEM results. As a demonstrator a life-size cantilever chair “Cellular Loop” has been developed and manufactured. The approach presented resulted in a loading capacity sufficient for everyday use. The procedure was filed for an application for a patent (Ziegler, Koplín and Jaeger 2012). It is applicable to any material and many technologies for additive manufacturing.

## Acknowledgments

The project is funded by the German Federal Ministry of Education and Research (Grant ID: 01RB0906A) under their BIONA program. We thank Dr. Gerken from rpm GmbH for the production of the test specimens and the chair.

## References

- Ajoku U, Saleh N, Hopkinson N, Hague R, and Erasenthiran P. (2006) Investigating mechanical anisotropy and end-of-vector effect in laser-sintered nylon parts. *Proc. IMechE, Part B: J. Engineering Manufacture*, 220(7), 1077–1086.
- Bernotat A (2013) Cellular Loop: Ein Freischwinger, entwickelt nach dem Vorbild der Natur. *Bautechnik*, 90(12), 777-782.
- Bruns A (2005) Numerische Untersuchung zum Tragverhalten von dünnwandigen, zylindrischen, zellulären Strukturen unter axialer Belastung, Diplomica Verlag GmbH, Hamburg, ISBN-13: 978-3838689852
- Caulfield B, McHugh P E, Lohfeld S (2007) Dependence of mechanical properties of polyamide components on build parameters in the SLS process. *Journal of Materials Processing Technology*, 182(1), 477-488.
- Chen Y (2006) A Mesh-Based Geometric Modeling Method for General Structures. *Proceedings of DETC'06 ASME Conference Philadelphia, Pennsylvania, September 10-13, 2006.*
- Cook D, Knier B, Gervasi V, Stahl D (2010) Automatic Generation of Strong, Light, Mutli-Functional Structures from FEA Output. *Proceedings of the 21st Annual International Solid Freeform Fabrication (SFF) Symposium. Austin (TX), USA (2010)*
- DCS Simulia. Abaqus 6.12 analysis user's manual. Abaqus 6.12 Documentation, 2011.
- Fratzl P (2007) Biomimetic materials research – what can we really learn from Nature's structural materials? *J. R. Soc. Interface*, 4:637–642
- Gibson L J (2005). Biomechanics of cellular solids. *Journal of biomechanics*, 38(3), 377-399.
- Goodridge R D, Tuck C J, Hague R J M (2012) Laser sintering of polyamides and other polymers. *Progress in Materials Science*, 57(2), 229-267.
- Hashin Z, Shtrikman S (1963) A variational approach to the theory of the elastic behaviour of multiphase materials. *J Mech Phys Solid* 11:127–140
- Hill R (1963), Elastic properties of reinforced solids: some theoretical principles., *J Mech Phys Solids* 11:357–372.
- Hjelm H E (1992) Elastoplasticity of Grey Cast Iron, FE-Algorithms and Biaxial Experiments. *Dissertation Chalmers University of Technology, Sweden*
- Hori M, Nemat-Nasser S (1999) On two micromechanics theories for determining micro-macro relations in heterogeneous solids. *Mech Mat* 31:667–682
- Kaddar W, Witt G (2010) Die Festigkeit in Abhängigkeit von Scanstrategien &-optionen beim Lasersintern vom Kunststoff. *Navigation*, 7, 8.
- Kowalczyk P (2003) Elastic properties of cancellous bone derived from finite element models of parameterized microstructure cells. *J Biomech*, 36:961-972
- Nunan K, Keller J (1984) Effective elasticity tensor of a periodic composite. *J Mech Phys Solid* 32:259–280.

- Oxman N (2011) Variable property rapid prototyping. *Virtual Phys. Prototyp.* 6:3–31
- Petrovic V, Haro JC, Jordá O, Delgado J, Blasco JR, Portolés L (2010) Additive Layered Manufacturing: Sectors of industrial application shown through case studies. *Int. J. Prod. Res.* 49:1061-1079.
- Ponche R, Kerbrat O, Mognol P, Hascoët J Y (2014) A novel methodology of design for Additive Manufacturing applied to Additive Laser Manufacturing process. *Robotics and Computer-Integrated Manufacturing*, 30(4), 389-398.
- Rosen D W (2007) Design for additive manufacturing: a method to explore unexplored regions of the design space. In *Eighteenth Annual Solid Freeform Fabrication Symposium* (pp. 402-415).
- Rowe N P and Speck T (2004) Hydraulics and mechanics of plants: novelty, innovation and evolution. *The Evolution of Plant Physiology* ed. A R Hemsley and I Poole (London: Academic) 301–29
- Schmid M (2015) *Selektives Lasersintern (SLS) mit Kunststoffen: Technologie, Prozesse und Werkstoffe*. Carl Hanser Verlag GmbH Co KG. ISBN: 978-3-446-44562-8
- Speck T and Rowe N P (2006) How to become a successful climber—mechanical, anatomical, ultra-structural and biochemical variations during ontogeny in plants with different climbing strategies. *Proc. 5th Int. Plant Biomechanics Conf.* (Stockholm: STFI Packforsk AB) 1:103–108
- Teufelhart S, Reinhart G (2012) Optimization of Strut Diameters in Lattice Structures. *Proceedings of the 23<sup>rd</sup> Annual International Solid Freeform Fabrication (SFF) Symposium*. Austin (TX), USA (2012)
- Van Hooreweder B, De Coninck F, Moens D, Boonen R, Sas P (2010) Microstructural characterization of SLS-PA12 specimens under dynamic tension/compression excitation. *Polymer testing*, 29(3), 319-326.
- Ziegler T, Koplin C, Jaeger R (2012) Verfahren zur Konstruktion mechanischer Komponenten. Patent DE-102012203869.8 (2012) und EP13158226.4 (2013)